Fracture Mechanics of Concrete Structures, de Borst et al (eds) © 2001 Swets & Zeitlinger, Lisse, ISBN 90 2651 825 0

Three-dimensional Numerical Concrete applied to investigate effective properties of composite materials

T.Hörsch & F.H.Wittmann
Institute for Building Materials, Swiss Federal Institute of Technology, ETH Hoenggerberg, Zurich

ABSTRACT: A three dimensional numerical model for the composite structure of concrete is proposed. Aggregates are embedded in a mortar matrix. The Interfacial Transition Zone (ITZ) between matrix and aggregates is also taken into consideration as a third phase. A finite element mesh generation of this model is realised by tetrahedral elements based on Delaunay triangulation. The aggregates, following a predefined size distribution, are placed randomly in the specimen. An increase of the aggregate concentration is possible but at the expense of the topological quality of the numerical model. The shape of the aggregates is approximated by spheres or ellipsoids. The matrix , consisting of mortar with a maximum grain-size of 2 mm, is assumed to be homogeneous with effective material parameters. The interface layer surrounding the aggregates represents a weak zone and can be assigned with statistically distributed material properties. Finite elements with linear or quadratic interpolation functions are considered. By means of this numerical model the effective properties and behaviour of the composite structure, e.g. the effective Poisson's ratio, are studied as function of parameters of its components. Furthermore time-dependent phenomena such as drying and stresses induced by hygral variations are simulated. The implementation of non-linear material laws and the smeared crack model enable the calculation of damage and crack formation in the specimen. As a final step the mechanical behaviour under coupled, external mechanical and hygral stresses is mentioned.

1 INTRODUCTION

The determination of the effective mechanical properties of a composite material like concrete by means of a numerical model require the consideration of at least the aggregates and the mortar matrix. Furthermore the implementation of the so called Interfacial Transition Zone (ITZ) between the aggregates and the mortar matrix is more realistic, because it can be regarded as the weak zone of the composite (Larbi 1993). Thus, the influence of each of the components on the global behaviour and the crack propagation can be investigated. The finite element model as well as the analysis and the implementation of the non-linear material laws, realized with the „semi-open" MARC program, are shortly described. A subdivision into "Numerical Model" for the discretization method and "Material Model" for the constitutive behaviour and the statistic distribution was choosen. Different numerical results obtained by the model when subjected to mechanical loading and time-dependent effects are outlined. The dependency of the analysis on the introduction of the Interfacial Transition Zone and statistically distributed material properties are shown by means of one test model with fixed dimensions lx, ly and lz.

2 NUMERICAL MODEL

2.1 *Generation*

The generation of the three-dimensional numerical model for concrete can be subdivided into two steps. First, the geometric construction of the specimen including a certain aggregate content and afterwards the meshing with finite elements.

2.2 *Topology of the model*

The numerical model reproduces a cubic specimen of mortar with randomly distributed aggregates according to the Fuller curve. The mortar is assumed to be homogeneous with effective material parameters. The aggregates are approximated by spheres or ellipsoids and their minimum diameter is 2 mm. These aggregates are placed successively in the specimen including checks of overlapping and exterior spacing. This was realized by adapting an existing C++ algorithm (Slowik, Leite 1999) to the developped program. An ITZ around each aggregate can be added.

2.3 *Meshing and element technology*

After that the geometric model will be meshed with four-node tetrahedron finite elements based on the

incremental Delaunay algorithm. The detailed background of this method was described e.g. by George and Borouchaki (1998). Hence, only a few remarks concerning typical properties and problems of the meshed model are described.

After the regular surface-meshing of the outsides of the specimen and the surfaces of the aggregates the construction of the spatial mesh is realised by incremental node-insertion. The criterion of an valable tetrahedral element is an extension of the well known two-dimensional Voronoi diagram and its dual, the Delaunay triangulation (Fig. 1). The method of field point insertion is more difficult as in two dimensions. While in two dimensions evenly well distributed nodes in the control space involve a mesh of finite elements with good shape quality, this is not necessary the case in three dimensions. The extreme case represents a tetrahedron, which fulfils the circumsphere criterion (Fig. 1) but its four nodes are coplanar. Hence, algorithmic steps have to be taken, so that the mesh quality does not fall below a special defined criterion. The regularity of the mesh can be defined as:

$$0 < \kappa^{-1} \leq \frac{\min d_C}{\max d_i} \leq \kappa < \infty \qquad (1)$$

where the constant κ is independent of the mesh and governs the ratio of the minimum circumference diameter d_c and the maximum inner sphere diameter d_i (Fig. 2). As a consequence of these problems the difficulties to observe the regularity of the FE-mesh increases with the complexity of the geometry and the control space respectively. A specimen with high aggregate content is much more delicate with respect to distorted elements.

The convergence of the numerical solution strongly depends on the regularity of the finite elements. Hence, the numerical model is limited concerning the aggregate content in order to achieve acceptable results. Up to now, aggregate contents up to 0.4 have been realized. Higher contents require an extremely fine mesh with the usual consequences for the computation time and the memory demand.

While generating the model in the observed way four-node isoparametric tetrahedral elements are used for the discretization of the system. The interpolation functions of these elements can be described as follows:

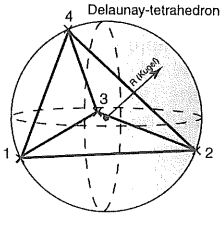

Figure 1: circumference criterion for a valid tetrahedron element

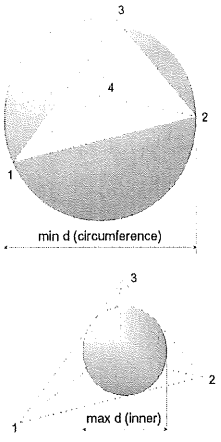

Figure 2: Criterion for the element regularity.

$$N_1 = 1-\xi-\eta-\zeta \quad N_2 = \xi \quad N_3 = \eta \quad N_4 = \zeta \qquad (2)$$

with the local axes ξ, η, ζ . The element stiffness integral is solved with the Gaussian quadrature formula and one integration point. This element shows poor bending behaviour and can cause locking problems (Groen & de Borst 1997). The assumed-strain concept offers the possibility to improve the element behaviour without raising the order of the shape functions (p-adaptivity). Thereby an enhanced strain field without even the requirement of C^0-continuity is added (Simo & Rifai 1990).

In this case the method of p-adaptivity was applied. After the mesh generation each element can be refined according to his interpolation functions as:

$$N_i = f(\xi, \eta, \zeta, \xi\eta, \xi\zeta, \eta\zeta, \xi N_1, \eta N_1, \zeta N_1) \qquad (3)$$

(Fig. 3). This element has ten nodes and four Gaussian integration points. The behaviour especially at hydrostatic pressure and for variable tangent stiff-

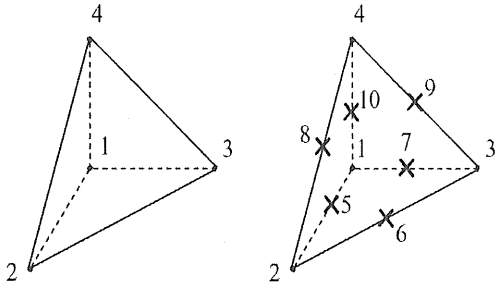

Figure 3: The two types of applied tetrahedron elements

ness matrices because of non-Hooke material law is improved. The additional computational cost of this refinement has not to be underestimated but it is justified in case of physical nonlinearity.

3 MATERIAL MODEL

3.1 *General remarks*

On displacement-controlled loading, concrete shows in both, the tension and the compression failure regime, an after peak behaviour, the so-called softening. The tensile strength of concrete depends on the biaxial stress state (Kupfer et al.1969) or the triaxial stress state (van Mier 1984) respectively. For the triaxial stress state the compression strength can increase up to more than three times the uniaxial value (van Mier 1984). The simulation of all these possible failure modes is a very complex problem. One advantage of the Numerical Concrete in this context is the fact, that comparatively simple material laws can be introduced on the mesolevel and the phenomenologically described and observed behaviour results from a rigorous analysis.

3.2 *The mortar matrix*

The mortar represents the cement paste including aggregates smaller than 2 mm. For the mortar matrix of the Numerical Concrete a smeared cracking model (Hillerborg 1983) for tension range in combination with a Drucker-Prager flow rule for the compression range is used. The total strain ε_{ij} is obtained by adding the elastic part ε^{e}_{ij} and the cracking or plastic part ε^{cp}_{ij}:

$$\varepsilon_{ij} = \varepsilon^{e}_{ij} + \varepsilon^{c,p}_{ij} \tag{4}$$

The softening curve, after reaching the cracking strain ε_{cr} , is modelled by an exponential function (Fig. 4):

$$\sigma(\varepsilon) = f_{ct} \cdot \exp(-\frac{\varepsilon_{cr}}{\varepsilon_{tu}}) \tag{5}$$

where f_{ct} = tensile strength; ε_{cr} = cracking strain; ε_{tu} = damage parameter. This function leads to less numerical problems than the bilinear representation of the curve and is more realistic than the linear softening.

As the exponential softening does not touch the x-axis, a limit value of the cracking strain was introduced to define the zero-stiffness at this point and direction:

$$\varepsilon^{\max}_{cr} = \frac{6 \cdot G_f}{f_{ct} \cdot h} \tag{6}$$

where G_f = fracture energy; f_{ct} = tensile strength; h = characteristical element length.
As mortar shows a more brittle behaviour than concrete, the fracture energy G_f was assumed to be 0.08 N/mm (Slowik 1995).

The identification of the characteristic element length h in case of tetrahedron elements can not be well-defined. The generated mesh implies finite elements with different dimensions. To simplify this problem the value of h is defined to the diameter of the maximum insphere of each element. Therefore there exists an integral measure for the shape of each tetrahedron.

If all principal stresses are positive, the failure criterion corresponds to the Rankine theory. The dependence of f_{ct} on negative principal stresses is considered by a linear decrease of f_{ct} down to 0.3 f_{ct}.

After the development of a fictitious crack at an integration point, at most two further cracks can develop, (orthogonal fixed crack model. This is not quite realistic, because of the loss of symmetry of the element stiffness. An improvement would be the implementation of a threshold angle α for the development of new fictitious cracks at the integration point.

The shear retention of a degraded zone is taken into account by a factor β. The dependence of the shear stiffness on the cracking strain is modelled by a linear decreasing shear retention factor β. β is zero at the state ε_{cr} = max ε_{cr}. This state is equal to a real crack.
A further case is the modelling of unloading during the softening range. According to experimental results a plastic fracturing behaviour was implemented (Chen et al. 1994). The degradation of the stiffness as function of the softening stress is modelled by a linear function (Fig. 5).

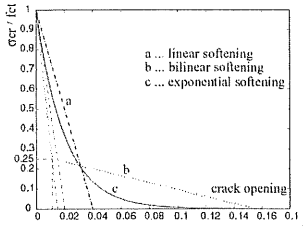

Figure 4: Numerical approximations of the softening curve

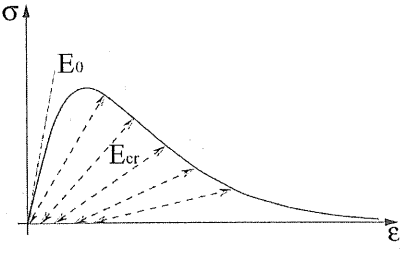

Figure 5: Qualitative gradient of the unloading state

The observation of typical stress-strain curves for concrete under compression shows three deformation segments. Roughly until 30% of f_c the σ-ε behaviour can be regarded as linear elastic. For higher stresses up to 70%-80% bond cracks develop and a resulting stiffness degradation is observed. Until the peak stress f_c a significant increase of the volume and strain takes places. The failure can be described as buckling and crushing.

The applied Drucker-Prager model can be described as follows:

$$f = \sqrt{J_2} + \alpha \cdot I_1 - k = 0 \tag{7}$$

where J_2 = second invariant of the deviatoric stress tensor; I_1 = first invariant of the stress tensor ; α, k = calibration factors. The initial failure surface begins at 30% of f_c, which terminates the elastic region. An isotropic hardening rule defines the plastic flow until the crushing state has been reached. A characterization of this strain state can be realized with e.g. the equivalent plastic strain:

$$\bar{\varepsilon}^{p} = \sqrt{\frac{2}{3}\,\varepsilon_{ij}^{p}\,\varepsilon_{ij}^{p}} \tag{8}$$

where ε^p_{ij} = the plastic strain tensor.

The limit states depend on J_2 and I_1 (Fig. 6). The observed post-peak region of concrete with softening and crack band localization is not implemented. The released fracture energy G_c for mortar is smaller than for concrete. The global behavior of the specimen for softening in compression results from the interaction with the aggregates.

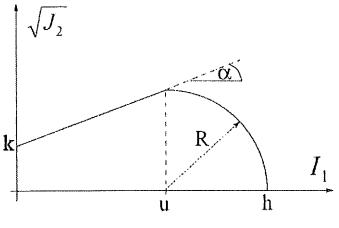

Figure 6: Drucker-Prager cap model in $I_1 - J_2^{1/2}$ plane

3.3 *The Interfacial Transition Zone (ITZ)*

The principal material behavior is equal to the mortar matrix. However the ITZ is a weak zone with higher porosity and lower strength than the mortar (Table 1).

The thickness of the ITZ was determined to be 0.2 mm. This value is an upper limit if compared with observations (Larbi 1993), but it is convenient concerning the meshing of the model.

3.4 *The aggregates*

The chosen material properties of the aggregates are typical for metamorphic rocks (Wittmann 1994). However, it has to be mentioned that in normal concrete several types of aggregates can be found which may complicate the simulation.

A summary of the mean material properties of the complete model is listed in Table 1.

3.5 *Statistically distributed material properties*

In order to approximate the real material property of concrete it is reasonable to introduce distributed values for the components. A usual method is the variation according to the Gaussian normal distribution. For the Numerical Concrete model such a distribution was implemented for the tension strength with a maximum spectrum of +/- 20%.

Table 1. Mean material properties of the components of the Numerical Concrete

	Matrix	ITZ	Aggregates
Young's modulus [N/mm^2]	15000	12000	60000
Poisson's ratio [-]	0.2	0.2	0.22
Tensile strength [N/mm^2]	3.0	2.0	15.0
Uniaxial compressive strength [N/mm^2]	30.0	20.0	200.0
Specific fracture energy [N/mm]	0.08	0.04	0.2
Coefficient of thermal expansion [-]	10^{-5}	10^{-5}	$9*10^{-6}$
Thermal conductivity [J/mm h K]	6.5	6.0	10.0
Specific heat [J/mm^3 K]	$2.4*10^{-3}$	$2.4*10^{-3}$	$2.1*10^{-3}$
Thermal film coefficient [J/mm^2 h]	0.15	-	≈ 0
Diffusion coefficient [mm^2/h]	2.0	2.2	≈ 0
Hygral film coefficient [kg/mm^2 h]	0.5	-	≈ 0

(Thermal properties will be used in the following extension of the model).

The specific fracture energy G_f was supposed to be linearly dependent on the tensile strength, as can been shown in experiments (Slowik 1995). The

Young's modulus can be determined according the CEB-FIP model code 1990 as:

$$E = E_{co} \cdot \left(\frac{\left(\frac{f_{ctm}}{0.3} \right)^{\frac{3}{2}} + \Delta f}{f_{cmo}} \right)^{\frac{1}{3}} \quad (9)$$

where E_{co} = referenz value; f_{ctm} = mean value of tension strength; $\Delta f = 8$ N/mm^2; $f_{cmo} = 10$ N/mm^2.

4 TEST SPECIMEN

The calculations were performed with small cubic specimens. The length is 10 mm and three aggregates were placed into the specimens with a resulting aggregate content of 0.28 (Fig.7). The simulation can be regarded as a sort of patch test for the model. Variation parameters of the model are the order of FE interpolation functions as well as constant and statistically distributed material parameters.

Limitations of the specimen size are determined by the computing capabilities. Figure 8 shows a more complicated Numerical Concrete model for further simulations.

5 MECHANICAL LOADING

The modeling of this problem can be described with the linearized elasticity theory as:

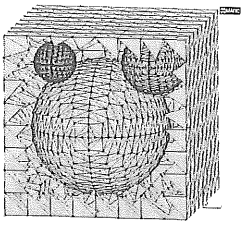

Figure 7: Numerical Concrete model used for the simulations.

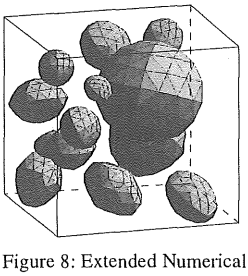

Figure 8: Extended Numerical Concrete model

$$div\ \sigma[\underline{u}] = \underline{f} \quad in\ \Omega \quad (10)$$

The constitutive equation and the boundary conditions are formulated as follows:

$$\sigma[\underline{u}] = \underline{\underline{D}}\ \varepsilon[\underline{u}] \quad (11)$$

$$\underline{u} = \underline{0} \quad on\ \Gamma_D = \partial\Omega \quad (Dirichlet) \quad (12)$$

$$\sigma[\underline{u}] \cdot \underline{n} = \underline{g} \quad on\ \Gamma_N = \partial\Omega \neg \Gamma_D \quad (Neumann) \quad (13)$$

For the finite element discretization the minimization of the residual leads to the weak form:

$$\int_\Omega \varepsilon[\underline{v}] : \sigma[\underline{u}]\, dV - \int_\Omega \underline{f}\, \underline{v}\, dV - \int_{\partial\Omega} \underline{g}\, \underline{v}\, dA = 0 \quad (14)$$

where v = valid virtual displacements. As mentioned, the stiffness matrix is not constant and the equations are solved incrementally using the rate form. The stresses are computed by the Total Lagrange formulation. For large displacements and strains the second Piola-Kirchhoff stress tensor and the Green-Lagrange strain tensor are used in the variational formulation of Equation 14.

After first linear elastic calculations and validations with analytical solutions had been carried out, uniaxial direct tension tests under displacement controlled conditions are now proposed. The deformation towards the z-axis was increased steadily and the xy-surfaces are fixed in plane.

Therefore three calculations were carried out with specific properties of the model as shown in Table 2:

Table 2. Characterization of the models

	Specimen 1	Specimen 2	Specimen 3
Dimensions [mm]	10x10x10	10x10x10	10x10x10
Aggregate content	0.28	0.28	0.28
ITZ	-	X	X
Statistic. dist. Prop. of the ITZ	-	-	X

Figures 9-11 show the degradation of the three models at the same "load" level of 150% of the mortar cracking strain. The effective Poisson's ratio for this case is about 0.14. The ficticious cracks develop mainly in the forced displacement direction, so the Poisson's ratio decreases. This is analogous to the increase of ν for uniaxial compression, because of the degradation lateral to the compression direction. As expected the degraded zones are near the aggregates. The influence of the ITZ on the crack band localization developping near the limit state is considerable, although in this simple case the failure region is obvious.

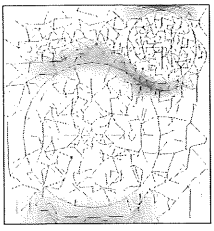

Figure 9: Ficticious cracks in a section of the model subjected to direct tension of specimen 1.

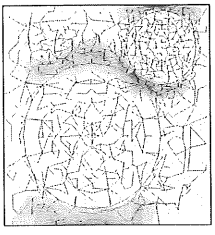

Figure 10: Ficticious cracks in a section of the model subjected to direct tension of specimen 2.

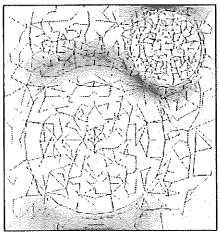

Figure 11: Ficticious cracks in a section of the model subjected to direct tension of specimen 3.

6 TIME DEPENDENT PHENOMENA

6.1 *Drying*

The drying process of a concrete specimen leads to hygral gradients from the outside to the centre. As the aggregates are nearly dense, the drying of the cement paste is hindered. The resulting moisture distribution is non-uniform and time-dependent. Drying, assymptotically reaches an equilibrum. The numerical simulation of this process shows the influence of the aggregate content on the drying process and the effective difussivity.

The governing equations of the drying process can be described with the second Fick's law:

$$\frac{\partial \underline{h}}{\partial t} - div[\underline{D}(\underline{h})\ grad\ \underline{h}] = Q(\underline{x},t) \qquad (16)$$

where m = mass flow, h = moisture potential , D(h) = moisture diffusion coefficient, Q(x,t) = source term.

The boundary conditions can be subdivided into Dirichlet and Neumann conditions:

$$\underline{h} = \bar{\underline{h}}(\underline{x},t) \qquad (17)$$

$$-\lambda \frac{\partial \underline{h}}{\partial \underline{n}} = f(\underline{h} - \underline{h}_0) \qquad (18)$$

where equation (18) describes the moisture transfer to the outside. The Dirichlet condition (17) is physically not very meaningful. The initial conditions are:

$$\underline{h}(\underline{x}, t = 0) = \underline{h}_i(\underline{x}) \qquad (19)$$

The humidity dependence of the diffusion coefficient can be described e.g. by an exponential function. From fitting of experimental results, the diffusion coefficient is obtained as:

$$\underline{D}(\underline{h}) = \alpha \cdot \exp(\beta \cdot \underline{h}) \qquad (20)$$

Hence, the variational form for the Finite Element Method can be described as:

$$\int_\Omega \underline{v} \frac{\partial \underline{h}}{\partial t} dV - \int_\Omega \underline{v}\, \underline{D}(\underline{h})\ \Delta \underline{h}\, dV - \int_\Omega \underline{Q}\, \underline{v}\, dV = 0 \qquad (21)$$

where v = valid virtual test function.
The coefficients α = 0.015 and β = 4.8 of Equation 20 are assigned to the diffusion coefficient of the mortar matrix (Wittmann et al. 1989). Figure 13 shows the experimentally determined curves for the diffusion coefficient. The aggregates are supposed to be dense. As initial condition the mortar matrix is fully saturated. No additional source terms are implemented, so that Equation 16 describes the loss of humidity of the specimen as a function of time and the diffusion coefficient D(h). Autogenous drying is not taken into consideration. The calculations were performed on one eigth of the model, taking the symmetry of the specimen into consideration (Fig. 12). Hence, the initial dimensions of the whole model are constant and L=20 mm.

Four calculations without cracking have been carried out. First, drying of a mortar cube to an environment with h=0.5 has been simulated. In this case it was assumed that five surfaces are sealed and drying is possible through the upper surface only. The moisture distribution after a drying time of about 2 hours in one eigth of the drying cube is shown in Figure 14a. The moisture potential is indicated by different levels of grey. The surface is in equilibrum with h=0.5 while the centre is still saturated (h=1). Then, aggregates have been placed in the mortar with three different volume concentra-

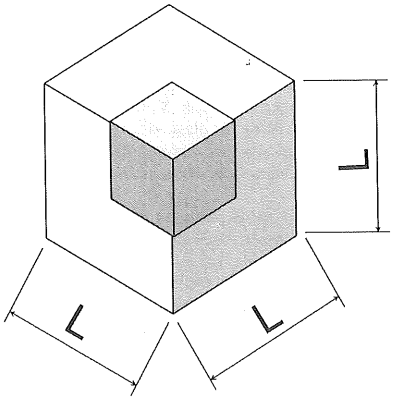

Figure 12: Eigth symmetry of the calculated drying model

tions. One eigth of the cube with the highest volume concentration is shown in Figure 14b. The retarding effect of aggregates on the drying proces can be clearly seen. Based on the former simulations, the

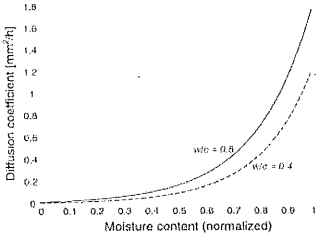

Figure 13: Diffusion coefficient as function of moisture content of concrete

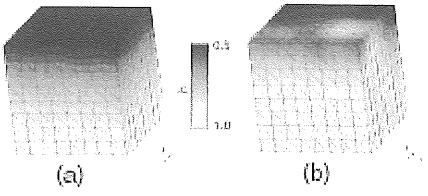

Figure 14: Drying of a mortar (a) and a concrete specimen (b).

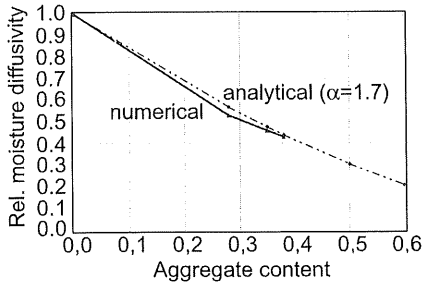

Figure 15: Normalized moisture diffusivity in terms of the aggregate content.

relative moisture diffusivity as function of the aggregate concentration has been determined and is plotted in Figure 15. The numerical results are compared with a power function (Equ. 22) for the diffusivity as function of the aggregate content.

$$D_{eff} = D_m \cdot (1-g)^{\alpha} \tag{22}$$

where D_{eff} = effective diffusivity, D_m = mortar diffusivity, g = aggregate content, α = 1.3 – 1.7 as factor for concrete. Obviously, the retardation effect of the whole drying process depends not only on the aggregate content, but also on the size distribution.

6.2 *Shrinkage*

The drying process results in a time-dependent moisture distribution in the composite material. As the moisture content decreases by Δh, shrinkage strains ε_s will occur. As a first approximation shrinkage of the cement-based matrix can be described with a constant coefficient of shrinkage as:

$$\varepsilon_s = \alpha_s \cdot \Delta h \tag{23}$$

As the aggregates are supposed to be dense, they will not undergo any shrinkage. As a consequence shrinkage of the mortar matrix is hindered by the aggregates and time-dependent eigenstresses are the result.

For this simulation a coupled analysis was used. The resulting stresses, induced by hygral gradients, are calculated within each time step. The symmetry of the model is taken into consideration. The specimen is not sealed so that drying through all sides is possible. The shrinkage coefficient of the mortar matrix was chosen to be constant: α_s = 0.002. The saturated specimen was supposed to be stored at a constant relative humidity (RH) of 50% . The diffusion coefficient as function of the the moisture content was modelled as shown in Figure 13.

A qualitative distribution of ficticious cracks after a drying time of 4 hours in four sections is shown in Figure 16. The dark zones represent the maximum cracking strains. The influence of the aggregate content and the size distribution on the crack formation and the possible crack closure during the drying period will be observed in the future. Another parameter to be varied will be the elastic modulus.

7 CONCLUSIONS

The Numerical Concrete is a suitable tool to investigate the effective properties of concrete as a composite material. By systematic variation of different component properties, it is possible to define the influence of each of them with respect to the global behaviour. This advantage as compared to phenomenological models for concrete is obtained at the

expense of a complex geometrical model and the size limitations.

The first observations of mechanical and time-dependent problems lead to a wide spectrum of applications of the 3-dimensional Numerical Concrete model.

8 OUTLOOK

The evaluation of effective properties of a composite material like concrete requires many calculations with a systematic variation of single parameters. Furthermore, extended models (Fig. 8) will have to be considered in the future.

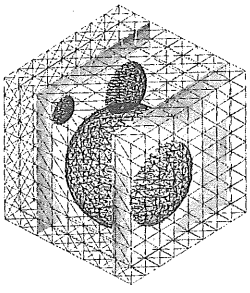

Figure 16: Fictitious crack formation in two sections of the model subjected to drying shrinkage

In the present analysis effective values have been chosen for the properties of the mortar matrix. In the future a stepwise approach will be chosen. First, hardened cement paste will be studied with fine inclusions only. The obtained effective values serve as properties for the matrix of mortar with coarser aggregates. Step by step this procedure can be repeated until the diameter of the maximum aggregate is reached.

The coupling of the two investigated loading types, i.e. mechanical load and drying shrinkage leads to a more realistic characterization of creep, shrinkage and failure under sustained load of concrete. Strains and crack formation induced by shrinkage and different additional mechanical loading will be investigated in detail.

REFERENCES

Chen, W.F. 1984. Constitutive equations for engineering materials – plasticity and modeling, Vol. 2. In I. Elishakoff (ed.), *Studies in applied mechanics 37B*. Elsevier, Amsterdam.

George, P.L. & Borouchaki, H. 1998. Delaunay triangulation and meshing. Application to Finite Elements. Hermes.

Groen, A.E. & de Borst, R. 1997. Three-dimensional Finite Element analysis of tunnels and foundations. Heron, Vol. 42, No. 4:183-214.

Hillerborg, A. 1983. Analysis of one single crack. In F.H. Wittmann (ed.). *Fracture mechanics of concrete*: 223-249. Elsevier, Amsterdam.

Kupfer, H.B. & Gerstle, K.H. 1973. Behaviour of concrete under biaxial stress. *Journal of Engineering Mechanics Div.* ASCE, EM4: 853-866.

Larbi, J.A. 1993. Microstructure of the Interfacial Zone around aggregate particles in concrete. Heron, Vol. 38, No. 1.

Simo, J.C. & Rifai, M.S. 1990. A class of mixed assumed strain methods and the method of incompatible modes. *International Journal for Numerical Methods in Engineering*. Vol. 29: 1595-1638.

Slowik, V. 1995. Beiträge zur experimentellen Bestimmung bruchmechanischer Parameter von Beton. In F.H. Wittmann (ed.). *Building Material Reports No.3*. Aedificatio, IRB.

Slowik, V. 1999. Modellierung des mechanischen Verhaltens von Betonen auf der Ebene des Mesogefüges. *Abschlussbericht 31.08.1999*, DFG. HTWK Leipzig. Fachbereich Bauwesen.

Van Mier, J.G.M. 1984. Strain softening under multiaxial loading conditions. *Thesis*. Eindhoven. University of Technology.

Wittmann, F.H. 1994. Relevante Werkstoffkenngrössen. In F.H. Wittmann (ed.). *Befestigte Fassadenelemente*. WTA-Schriftenreihe. Heft 4: 11-48. Aedificatio.

Wittmann, X.; Sadouki, H. & Wittmann, F.H. 1989. Numerical evaluation of drying test data. In A.H. Hadjian (ed.). *Transactions of the 10th international conference on structural mechanics in reactor technology*. (SMiRT). Vol. Q. Anaheim: 71-77.